



This is a repository copy of *Finite element analysis of the damage mechanism of 3D braided composites under high-velocity impact*.

White Rose Research Online URL for this paper:
<http://eprints.whiterose.ac.uk/112250/>

Version: Accepted Version

Article:

Zhang, C., Curiel-Sosa, J.L. and Duodu, E.A. (2017) Finite element analysis of the damage mechanism of 3D braided composites under high-velocity impact. *Journal of Materials Science*, 52 (8). pp. 4658-4674. ISSN 0022-2461

<https://doi.org/10.1007/s10853-016-0709-7>

The final publication is available at Springer via
<http://dx.doi.org/10.1007/s10853-016-0709-7>.

Reuse

Unless indicated otherwise, fulltext items are protected by copyright with all rights reserved. The copyright exception in section 29 of the Copyright, Designs and Patents Act 1988 allows the making of a single copy solely for the purpose of non-commercial research or private study within the limits of fair dealing. The publisher or other rights-holder may allow further reproduction and re-use of this version - refer to the White Rose Research Online record for this item. Where records identify the publisher as the copyright holder, users can verify any specific terms of use on the publisher's website.

Takedown

If you consider content in White Rose Research Online to be in breach of UK law, please notify us by emailing eprints@whiterose.ac.uk including the URL of the record and the reason for the withdrawal request.



eprints@whiterose.ac.uk
<https://eprints.whiterose.ac.uk/>

Finite element analysis of damage mechanism of 3D braided composites under high velocity impact

Chao Zhang*, Enock A Duodu, Xiaojing Xu

(School of Mechanical Engineering, Jiangsu University)

*Corresponding author: Chao Zhang, E-mail: zhangchao@ujs.edu.cn, Tel: +86 511 88780169, Fax: +86 511 88790627,

301 Xuefu Road, Zhenjiang, 212013, Jiangsu, China

Abstract: The integrated near-net-shape structure of 3D braided composites provides excellent impact resistant properties over laminated composites. At the same time, the load distribution and damage mechanisms throughout the structures become more complicated. In this paper, a finite element model based on three unit-cells is established to simulate the penetration process of 3D braided composites under high velocity impact. A 3D rate-dependent constitutive model is developed to determine the constituent behavior in the three unit-cells. Tsai-Wu criterion with Mises criterion and an instantaneous degradation scheme are coded by a user material subroutine VUMAT developed in Abaqus/Explicit. The whole process of ballistic damage evolution of 3D braided composites is simulated, and the impact resistance and damage mechanisms are revealed in detail in the simulation process. The effects of striking velocity on the ballistic properties and energy absorption characteristics of the composite structures are also discussed.

Keywords: 3D braided composites, Damage mechanisms, Finite element simulation, High velocity impact

1 Introduction

With the development of military science and technology, the damage capability of missiles and anti-aircraft weapons is improving continuously, which results in growing threats to military aircrafts. Therefore, it is important to involve survivability of personnel and equipment against penetration by high velocity projectiles before the application of new aeronautical materials.

In order to reduce the structural weight and increase the flexibility of the aircraft, laminated composites have been widely used in the aerospace industry because of their high performance-weight ratio. However, poor out-of-plane properties, low damage tolerance and low delamination resistance have restricted their applications in primary-loading components. Delamination is the main damage mechanism of laminated composites under ballistic impact, which can cause obvious degradation of the material mechanical properties. In recent years, 3D braided composites have received much attention due to their excellent advantages over the laminated composites. The distinct feature of 3D braided composites is integrated near-net-shape structure to provide outstanding through-thickness properties and prevent delamination under ballistic impact loading. Owing to these prominent merits, 3D braided composites are believed to have broad potential applications in military aircrafts, armor vehicles

and protective structures.

The quasi-static mechanical properties of 3D braided composites have been studied extensively, including the establishment of microstructure models [1-4], the prediction of stiffness and strength properties [5-8], and the investigation of damage and failure mechanisms under various static loadings [9-12]. However, thus far, the reports regarding the high velocity impact performance of 3D braided composites are relatively limited.

Some researchers conducted ballistic impact experiments to study the penetration resistance and damage mechanism of 3D braided composites. Gong and Sankar [13] experimentally analyzed the impact damage pattern of 3D braided composites and compared the impact tolerance between 3D braided composites and quasi-isotropic laminates. It is found that 3D braided composites show better damage tolerance than quasi-isotropic laminates with approximate bending stiffness in the primary direction. Flanagan et al. [14] carried out a high velocity impact experiment to investigate the damage mechanism in woven, 3D braided and needle punched composites under impact velocities ranging from 200 to 1100 m/s. The penetration resistance and failure modes of these different textile composites were analyzed and compared. Xu and Gu [15] explored the macro- and micro-fracture morphology of 3D braided composites after ballistic perforation by using scanning electron microscope (SEM). They concluded that the dominant failure mechanisms are shear and compression failures on the front side and fiber tensile failure on the back side of the target plate.

Physical impact experiments are expensive, time-consuming, and confined to certain structural parameters and certain impact conditions. Hence, the development of robust analytical and numerical modeling methods is essential to the structural design, optimization and application of 3D braided composites. Analytical studies are based on some simplified assumptions and mainly focused on the impact events of laminated composites [16], plain weave [17] and 3D orthogonal weave composites [18] with relatively simple microstructures. It is difficult to solve the impact problems of 3D braided composites with complex microstructure by theoretical analysis methods. However, less limitation exists in the impact simulation by using finite element method. Therefore, finite element modeling method is preferred by the researchers to study the impact damage of 3D braided composites.

Jenq et al. [19, 20] implemented an experimental and numerical study on the ballistic impact response of 3D two-step and four-step braided glass/epoxy composites. They first performed a quasi-static punch test to obtain the load-displacement curves and penetration damage modes of the target, and then incorporated them into the finite element penetration analysis of the composites. In the numerical model, 3D braided composites were considered as continuous anisotropic materials and meshed with various densities in different regions. The properties degradation of material after failure occurrence was determined by the quasi-static load-displacement curves and the corresponding regions in the specimen. Gu and Ding [21] adopted the 'fiber inclination model' proposed by Yang et al. [1] to replace the real microstructure of 3D braided composites and employed this model to calculate the residual velocity of projectile that perforated a 3D braided composite target. Comparisons between numerical results and experimental results validate the applicability of this quasi-microstructure model.

In the references [19-21], braided composites are modeled by the macroscopic method and treated as homogenized anisotropic materials thus the real microstructure can not be well reflected. To cover these intrinsic limitations, Ji and Kim [22] and Gu [23] established the actual microstructure of the 3D woven and braided composites in the scale of constituents. Thence, combined with different constitutive models for each constituent,

the whole impact processes were simulated and the specific mechanical responses of yarns and matrix were presented. Such a microscopic method is known as the direct numerical simulation (DNS). By this approach, the impact damage mechanism initiated in the microscopic scale and propagated to the macroscopic scale can be revealed in detail. However, applying DNS model needs tremendous computer memory and high-performance computing resource, which brings a huge obstacle for practical engineering applications.

The establishment of impact simulation model in the macroscopic scale while considering the microstructure of composites is an effective strategy. Through macroscopic modeling method, Bahei-El-Din and Zikry [24] analyzed the deformation fields and stress wave propagations in woven composites induced by different impact velocities. In their model, the orthotropic elastic constants of the composite target elements were derived from a microscopic unit-cell model. In the transverse impact simulation work conducted by Zhang et al. [25], an interior unit-cell model in which the yarns and matrix were explicitly modeled was developed to characterize the stiffness matrix and damage evolution of 3D braided composites. Similar studies dealing with the impact damage problems of other textile composites based on the unit-cell models can be found in references [26-28].

It is known that 3D braided composites have a skin-core structure and are composed of three regions: interior, surface and corner [3, 4]. Each region is built up of identical unit-cell with unique yarn configuration and distinctive properties which must be treated separately. However, previous work mostly neglected the surface and corner unit-cells but only adopted the interior unit-cell to establish the impact damage model. Meanwhile, the obvious rate-dependent characteristics of 3D braided composites under ballistic impact have not been studied well.

In this paper, a three unit-cells model is proposed to simulate the penetration process of 3D braided composites under high velocity impact. A 3D rate-dependent constitutive model, developed from the rheological model, is used to determine the constituent behaviors in the three unit-cells. Tsai-Wu failure criterion with various damage modes and Mises criterion are applied to predict damage initiation of yarns and matrix with an instantaneous degradation scheme. A user material subroutine VUMAT involving the constitutive equation and failure model is written and implemented in commercial finite element software ABAQUS/Explicit. The ballistic resistance and damage mechanisms of 3D braided composites are studied in detail. In addition, discussions are carried out to uncover the influences of striking velocity on the ballistic performance and energy absorption characteristics of the braided composite structures.

2 Microstructure analysis and three unit-cells model

The topological structure of 3D braided composites is determined by the movements of carriers on the machine bed and the connected motion mechanisms of braiding yarns. In the four-step braiding process, the surface and corner carriers move in distinctly different manner than the interior carriers. This is because the carriers in the top and bottom rows do not participate in any row movement and the carriers in the leftmost and the rightmost columns do not participate in any column movement [2]. Since the yarn configurations in the interior, surface and corner regions of the preform are unique, they should be treated separately.

The ‘jamming’ action will straighten and reposition the braiding yarns in space after a machine cycle. Considering that the braiding yarns expand $h/4$ at each step along braiding direction, the schematic of all the yarn paths projected into the x - y plane is presented in Fig. 1. Afterwards, in order to investigate the topological structure,

the control volume method is employed individually in different regions of 3D braided preform. A control volume is defined as a stationary volume in space into which yarns entering and leaving can be observed during the carrier's four-step movements. By adopting this method, the relationship between the braiding process and the resulting yarn topology can be demonstrated and three distinct types of unit-cells located in the interior, surface and corner regions of the preform can be determined. More detailed analysis can be found in our previous work [8].

Figure 1 also illustrates the selection of three unit-cells. These unit-cells are oriented in the same reference frame as the preform cross-section to facilitate the mechanical analysis. Figure 2 shows the topology geometrical models and the corresponding solid structure models of the three unit-cells.

In Fig. 2, γ , θ and β are the interior braiding angle, surface braiding angle and corner braiding angle, respectively. W and T indicate the width and thickness of the unit-cell models, under which sub-index i , s and c refer to the interior, surface and corner regions respectively. Obviously, the heights h of the three unit-cells are identical.

In practice, γ , θ and β are difficult to measure directly; however, they can be calculated by knowing the braiding angle α on the surface of the composites, as given by

$$\tan \alpha = W_i / h \quad (1)$$

$$\tan \gamma = \sqrt{2}W_i / h = \sqrt{2} \tan \alpha \quad (2)$$

$$\tan \theta = (W_i / 4\sqrt{2}) / ((3/8)h) = \tan \gamma / 3 \quad (3)$$

$$\tan \beta = \tan \theta \quad (4)$$

Consequently, once the braiding angle α and the pitch length h are determined, the topology geometrical models of the three unit-cells can be fully characterized.

3 Dynamic damage constitutive model

High velocity impact or ballistic impact is a transient dynamic process. The target response is governed by the local behavior of the material in a small region around the impact point, and is generally independent of its boundary conditions. That is, the impact-contact interaction is over before the stress waves reach to the target boundaries and return to affect the impact region. In this case, the target material always presents obvious rate-dependent behavior. Especially for composite materials, the influence of strain rate effect on the mechanical properties become very complicated due to the anisotropic characteristics.

3D braided composites are composed of braiding yarns and the resin matrix. The macroscopic mechanical behavior of the 3D braided composites under high velocity impact is determined by the microscopic constitutive relationships of the constituents. Generally, the resin matrix is assumed to be isotropic material; the braiding yarns are regarded as unidirectional composites and transversely isotropic materials in local coordinate. Consequently, establishing the rate-dependent constitutive equations of matrix and unidirectional composites is the premise for simulating the structural behavior of 3D braided composites under high velocity impact loading by three unit-cells model.

3.1 Constitutive model of carbon fiber and epoxy matrix

Based on the small deformation assumption, the carbon fiber is considered as rate-independent linear-elastic material and the epoxy matrix is considered as time-dependent linear-viscoelastic material. As shown in Fig. 3, a spring element is used to model the constitutive relationship of the fiber, and a rheological model of a spring in parallel with two Maxwell elements is used to express the constitutive relationship of the matrix. Their constitutive equations can be presented as follows:

$$\sigma_f = E_f \varepsilon \quad (5)$$

$$\sigma_m(t) = \int_0^t E_r(t-\tau) \dot{\varepsilon} d\tau \quad (6)$$

where E_f is the elastic modulus of the fiber, and E_r is the relaxation modulus of the matrix.

Under constant strain, $E_r(t)$ can be given as [29]:

$$E_r(t) = E_m + E_1 e^{\frac{-tE_1}{\eta_1}} + E_2 e^{\frac{-tE_2}{\eta_2}} \quad (7)$$

where E_m is the elastic modulus of the matrix under quasi-static condition; E_1 and E_2 are time-dependent modulus controlled by the dashpots with viscous coefficients η_1 and η_2 .

3.2 Rate dependent constitutive model for unidirectional composite

In the local coordinate system of unidirectional composite, the 1-axis indicates the fiber direction and the 2- and 3-axes are referred as the transverse directions. As shown in Fig. 4, the unidirectional composite loaded in the longitudinal direction can be modeled with elastic springs and Maxwell elements. A linear elastic spring, which represents the reinforced fiber, is parallel with the rheological model for the epoxy matrix. With the assumption of iso-strain, the stress-strain relationship for the unidirectional composite in the longitudinal direction can be expressed as

$$\bar{\sigma}_{11}(t) = \int_0^t E_{f1}(t-\tau) \dot{\varepsilon}(\tau) d\tau = V_f E_{f1} \varepsilon_{11} + (1-V_f) \int_0^t E_r(t-\tau) \dot{\varepsilon}_{11} d\tau \quad (8)$$

where E_{f1} is the Young's modulus of the fiber in longitudinal direction, and V_f is the fiber volume fraction of the composite.

Under constant strain rate, substituting the expression of $E_r(t)$ in Eq. (7) into Eq. (8) and setting $t = \varepsilon_{11} / \dot{\varepsilon}_0$, yields[29]:

$$\bar{\sigma}_{11}(\varepsilon_{11}) = (E_{f1} V_f + E_m (1-V_f)) \varepsilon_{11} + E_1 V_m \theta_{e1} \dot{\varepsilon}_0 \left(1 - e^{-\frac{\varepsilon_{11}}{\dot{\varepsilon}_0 \theta_{e1}}}\right) + E_2 V_m \theta_{e2} \dot{\varepsilon}_0 \left(1 - e^{-\frac{\varepsilon_{11}}{\dot{\varepsilon}_0 \theta_{e2}}}\right) \quad (9)$$

where $\dot{\varepsilon}_0$ is a constant strain rate, $\theta_{e1} = \eta_1 / E_1$ and $\theta_{e2} = \eta_2 / E_2$ are characteristic relaxation times in Maxwell elements. The first term on the right hand of Eq. (9) represents the elastic characteristic of the composite, and the remaining two terms reflect the strain rate effect on the constitutive relationship. If setting $V_f=0$, Eq. (9) just reduces to the rate-dependent constitutive relationship for the viscoelastic matrix.

Similarly, with iso-strain or iso-stress assumption, the constitutive relationships of unidirectional composite under other simple loads can be given by rule of mixtures as [29]:

$$\left\{ \begin{array}{l} \bar{\sigma}_{22}(\varepsilon_{22}) = \frac{E_{f2}E_m}{E_{f2}(1-V'_f) + E_mV'_f} \varepsilon_{22} + \dot{\varepsilon}_0 \frac{Q}{M} (1 - e^{-M \frac{\varepsilon_{22}}{\dot{\varepsilon}_0}}) + \dot{\varepsilon}_0 \frac{R}{N} (1 - e^{-N \frac{\varepsilon_{22}}{\dot{\varepsilon}_0}}) \\ \bar{\tau}_{12}(\gamma_{12}) = \frac{G_{f12}G_m}{G_{f12}(1-V'_f) + G_mV'_f} \gamma_{12} + \dot{\gamma}_0 \frac{Q_{12}}{M_{12}} (1 - e^{-M_{12} \frac{\gamma_{12}}{\dot{\gamma}_0}}) + \dot{\gamma}_0 \frac{R_{12}}{N_{12}} (1 - e^{-N_{12} \frac{\gamma_{12}}{\dot{\gamma}_0}}) \\ \bar{\tau}_{23}(\gamma_{23}) = \frac{G_{f23}G_m}{G_{f23}(1-V'_f) + G_mV'_f} \gamma_{23} + \dot{\gamma}_0 \frac{Q_{23}}{M_{23}} (1 - e^{-M_{23} \frac{\gamma_{23}}{\dot{\gamma}_0}}) + \dot{\gamma}_0 \frac{R_{23}}{N_{23}} (1 - e^{-N_{23} \frac{\gamma_{23}}{\dot{\gamma}_0}}) \end{array} \right. \quad (10)$$

In the above equations, E_{f2} is the Young's modulus of the fiber in transverse direction; $V'_f = \sqrt{V_f}$ is the modified fiber volume fraction of the composite; G_{f12} , G_{f23} are the shear moduli of the fiber in the 1-2 and 2-3 plane respectively; M , N , Q , R with sub-index 12 or 23 and without sub-index are parameters governed by the rheological model under various loading cases, and their expressions are given in reference [29] in detail.

According to the generalized Hook's law, the stress-strain relationship of orthotropic material is

$$\varepsilon = S\sigma \quad (11)$$

where S is the compliance matrix.

Define U and E^{-1} as:

$$U = \begin{bmatrix} 1 & -\mu_{21} & -\mu_{31} & 0 & 0 & 0 \\ -\mu_{12} & 1 & -\mu_{32} & 0 & 0 & 0 \\ -\mu_{13} & -\mu_{23} & 1 & 0 & 0 & 0 \\ 0 & 0 & 0 & 1 & 0 & 0 \\ 0 & 0 & 0 & 0 & 1 & 0 \\ 0 & 0 & 0 & 0 & 0 & 1 \end{bmatrix}, \quad E^{-1} = \begin{bmatrix} 1/E_{11} & 0 & 0 & 0 & 0 & 0 \\ 0 & 1/E_{22} & 0 & 0 & 0 & 0 \\ 0 & 0 & 1/E_{33} & 0 & 0 & 0 \\ 0 & 0 & 0 & 1/G_{23} & 0 & 0 \\ 0 & 0 & 0 & 0 & 1/G_{31} & 0 \\ 0 & 0 & 0 & 0 & 0 & 1/G_{12} \end{bmatrix}$$

One has

$$S = E^{-1}U \quad (12)$$

Then Eq. (11) can be rewritten as

$$\sigma = U^{-1}E\varepsilon \quad (13)$$

Therefore, the 3D rate-dependent constitutive relationship of unidirectional composite can be given by:

$$\left\{ \begin{array}{l} \sigma_{11} \\ \sigma_{22} \\ \sigma_{33} \\ \sigma_{23} \\ \sigma_{31} \\ \sigma_{12} \end{array} \right\} = U^{-1} \left\{ \begin{array}{l} \int_0^t E_{11}(t-\tau) \dot{\varepsilon}(\tau) d\tau \\ \int_0^t E_{22}(t-\tau) \dot{\varepsilon}(\tau) d\tau \\ \int_0^t E_{22}(t-\tau) \dot{\varepsilon}(\tau) d\tau \\ \int_0^t G_{23}(t-\tau) \dot{\varepsilon}(\tau) d\tau \\ \int_0^t G_{12}(t-\tau) \dot{\varepsilon}(\tau) d\tau \\ \int_0^t G_{12}(t-\tau) \dot{\varepsilon}(\tau) d\tau \end{array} \right\} = U^{-1} \left\{ \begin{array}{l} \bar{\sigma}_{11} \\ \bar{\sigma}_{22} \\ \bar{\sigma}_{33} \\ \bar{\sigma}_{23} \\ \bar{\sigma}_{31} \\ \bar{\sigma}_{12} \end{array} \right\} \quad (14)$$

3.3 Unit-cell homogenization

For the local coordinate definition of yarn in a specific orientation, local 1-axis follows the yarn centerline and local 3-axis is in the upright plane perpendicular to the X - Y plane of the global coordinate, as shown in Fig. 5.

Based on the iso-strain assumption, the strain matrix can be transformed from the global to the local coordinate system by:

$$\bar{\boldsymbol{\varepsilon}} = \boldsymbol{T}_\sigma^T \boldsymbol{\varepsilon} \quad (15)$$

where $\bar{\boldsymbol{\varepsilon}}$ and $\boldsymbol{\varepsilon}$ are the strain matrix in the local and global coordinates respectively; \boldsymbol{T}_σ is the transformation matrix of stress and expressed as follows:

$$\boldsymbol{T}_\sigma = \boldsymbol{T}_\sigma(\boldsymbol{\psi}, \boldsymbol{\varphi}) = \begin{bmatrix} l_1^2 & m_1^2 & n_1^2 & 2m_1n_1 & 2l_1n_1 & 2l_1m_1 \\ l_2^2 & m_2^2 & n_2^2 & 2m_2n_2 & 2l_2n_2 & 2l_2m_2 \\ l_3^2 & m_3^2 & n_3^2 & 2m_3n_3 & 2l_3n_3 & 2l_3m_3 \\ l_2l_3 & m_2m_3 & n_2n_3 & m_2n_3 + m_3n_2 & l_2n_3 + l_3n_2 & l_2m_3 + l_3m_2 \\ l_3l_1 & m_3m_1 & n_3n_1 & m_3n_1 + m_1n_3 & l_3n_1 + l_1n_3 & l_3m_1 + l_1m_3 \\ l_1l_2 & m_1m_2 & n_1n_2 & m_1n_2 + m_2n_1 & l_1n_2 + l_2n_1 & l_1m_2 + l_2m_1 \end{bmatrix} \quad (16)$$

where (l_i, m_i, n_i) are directional cosines. They are the cosines between direction of fiber yarns and axis of global coordinate system. $l_i = \cos(i, X)$, $m_i = \cos(i, Y)$, $n_i = \cos(i, Z)$, $(i=1,2,3)$.

Then, the stress matrix of a braiding yarn in the local coordinate can be calculated by Eq. (14). In the global coordinate, stress matrix can be computed by

$$\boldsymbol{\sigma} = \boldsymbol{T}_\sigma \bar{\boldsymbol{\sigma}} \quad (17)$$

where $\bar{\boldsymbol{\sigma}}$ and $\boldsymbol{\sigma}$ are the stress matrix in the local and global coordinates respectively.

The orientation of the yarns in the interior, surface and corner unit-cells can be characterized by different braiding angles $\boldsymbol{\psi}$ and horizontal orientation angles $\boldsymbol{\varphi}$, given as follow

$$\begin{cases} (\boldsymbol{\gamma}, \boldsymbol{\varphi}), (\boldsymbol{\gamma}, -\boldsymbol{\varphi}), (-\boldsymbol{\gamma}, \boldsymbol{\varphi}), (-\boldsymbol{\gamma}, -\boldsymbol{\varphi}) \\ (\boldsymbol{\theta}, \boldsymbol{\varphi}), (\boldsymbol{\theta}, -\boldsymbol{\varphi}), (-\boldsymbol{\theta}, \boldsymbol{\varphi}), (-\boldsymbol{\theta}, -\boldsymbol{\varphi}) \\ (\boldsymbol{\beta}, \boldsymbol{\varphi}), (\boldsymbol{\beta}, -\boldsymbol{\varphi}), (-\boldsymbol{\beta}, \boldsymbol{\varphi}), (-\boldsymbol{\beta}, -\boldsymbol{\varphi}) \end{cases} \quad (18)$$

For each unit-cell, its homogenized stress station can be calculated by volume averaging method, namely,

$$\boldsymbol{\sigma}_a = \sum_{n=\text{direction1}}^{\text{direction4}} v_n \boldsymbol{\sigma}_n + v_m \boldsymbol{\sigma}_m \quad (19)$$

in which, $\boldsymbol{\sigma}_a$ is averaging stress matrix corresponding to each unit-cell; $\boldsymbol{\sigma}_n$, $\boldsymbol{\sigma}_m$ are stress matrices of each inclined yarn and matrix ; v_n , v_m are the volume proportion of yarns in each orientation and the volume proportion of matrix in each unit-cell.

3.4 Failure initiation criteria

Damage initiation and damage evolution can be simulated by damage mechanism, which consist of failure criteria and material degradation. Actually, 3D braided composites comprise three phases: fiber yarns, epoxy matrix and interface. Therefore, the failure mechanism contains three types: yarn failure, matrix cracking and interface debonding. However, in this study, the damage mechanism of interface debonding is not considered.

Tsai-Wu criterion, implemented to predict the failure initiation of braiding yarn, is given by

$$F_{11}\sigma_1^2 + F_{22}\sigma_2^2 + F_{33}\sigma_3^2 + F_{44}\sigma_{23}^2 + F_{55}\sigma_{13}^2 + F_{66}\sigma_{12}^2 + 2F_{12}\sigma_1\sigma_2 + 2F_{13}\sigma_1\sigma_3 + 2F_{23}\sigma_2\sigma_3 + F_1\sigma_1 + F_2\sigma_2 + F_3\sigma_3 = 1 \quad (20)$$

In the above equation,

$$\begin{aligned} F_{11} &= \frac{1}{X_T X_C}, & F_{22} &= F_{33} = \frac{1}{Y_T Y_C}, \\ F_{44} &= \frac{1}{S_{23}^2}, & F_{55} &= F_{66} = \frac{1}{S_{12}^2}, \\ F_{12} &= F_{13} = -\frac{1}{2}\sqrt{F_{11}F_{22}}, & F_{23} &= -\frac{1}{2}\sqrt{F_{22}F_{33}}, \\ F_1 &= \frac{1}{X_T} - \frac{1}{X_C}, & F_2 &= F_3 = \frac{1}{Y_T} - \frac{1}{Y_C} \end{aligned}$$

where X_t and X_c are the axial tensile and compressive strengths of yarn; Y_t and Y_c are the transverse tensile and compressive strengths; S_{12} and S_{23} are the in-plane and out of plane shear strengths, respectively.

The static strength properties of braiding yarn can be calculated using the micromechanics formulae given by Chamis [30]. Herein, considering the strain rate effect on the mechanical properties of composite materials, the strength parameters appeared in Eq. (20) are modified by the rate dependent strength properties described as:

$$F = F_0 \left(1 + c \ln \frac{|\dot{\epsilon}|}{\dot{\epsilon}_0}\right) \quad (21)$$

where F is the current strength (tension, compression or shear) of composite in different loading direction, $\dot{\epsilon}$ is the corresponding strain rate, F_0 is the reference strength under reference strain rate $\dot{\epsilon}_0$, and c is the modification factor which can be determined by fitting the test data.

It is known that Tsai-Wu failure criterion is mode-independent. It identifies the failure initiation but cannot identify the failure modes of each braiding yarn. Thus, six indices, H_i ($i = 1-6$), are defined to identify the failure modes of the failed material, namely

$$\begin{aligned} H_1 &= F_1\sigma_{11} + F_{11}\sigma_{11}^2, & H_2 &= F_2\sigma_{22} + F_{22}\sigma_{22}^2 \\ H_3 &= F_3\sigma_{33} + F_{33}\sigma_{33}^2, & H_4 &= F_{44}\sigma_{23}^2 \\ H_5 &= F_{55}\sigma_{13}^2, & H_6 &= F_{66}\sigma_{12}^2 \end{aligned} \quad (22)$$

At failure, the maximum one of the six indices H_i ($i = 1-6$) is assumed to identify the dominant failure mode. Failure index H_1 indicates yarn longitudinal breaking, H_2 and H_3 indicate yarn transverse cracking, and H_4 , H_5 and H_6 indicate shear failure modes of yarn in 23, 13 and 12 planes.

The Mises criterion is adopted as matrix failure criterion, namely,

$$(\sigma_1 - \sigma_2)^2 + (\sigma_1 - \sigma_3)^2 + (\sigma_3 - \sigma_2)^2 + 6(\tau_{12}^2 + \tau_{23}^2 + \tau_{31}^2) = 2\sigma_{pm}^2 \quad (23)$$

where σ_{pm} is cracking strength of pure matrix.

4 Numerical simulation of high velocity impact

The Explicit module in ABAQUS software is used to establish the finite element model for analyzing the damage characteristics of 3D braided composites under high velocity impact. The finite element model is based on three different unit-cells: interior, surface and corner. The 3D rate dependent constitutive equation, failure initiation criteria and instantaneous degradation scheme described in the previous section are coded into a user-defined material subroutine (VUMAT) to compute the stress state and analyze the damage behavior in the three unit-cells. The region division of the 3D braided composite plate according to the three unit-cells model is displayed in Fig. 6. Here, z axis and y axis refer to the axial and thickness directions of the material.

4.1 Finite element model

In the numerical simulation, two different shapes of projectiles are used: spherical and flat cylindrical projectiles. The diameter of the spherical projectile is 8 mm; the diameter and height of the flat cylindrical projectile are 8 mm and 16 mm, respectively. The projectile is considered to be rigid body (analytical rigid) with center (reference point) of mass (6.27g) located such to coincide with the y -axis, and doesn't produce substantial distortion during the penetration process. The rotational inertia of the projectile is not necessary since the friction between the projectile and the target plate is ignored. The hourglass controlled eight-node C3D8R elements are used to discretize the 3D braided composite plate. The stress calculation at the integration points and the damage analysis in the interior, surface and corner regions of composite plate are based on three different unit-cell models.

In the high velocity impact penetration process, the deformation and damage of the target plate mainly occur in the contact zone. Accordingly, a gradual mesh generation method is adopted, and the mesh density decreases gradually from the impact point to the edges of the target plate. This mesh not only ensures the accuracy of the numerical results, but also improves the computation efficiency of the model.

Fig. 7 shows the finite element model of 3D braided composites under high velocity impact. In Fig. 7, z axis, x axis and y axis indicate the axial and two transverse directions of the material. The composite plate model consists of 82,320 nodes and 74,880 C3D8R elements.

4.2 Boundary condition and contact definition

Ballistic impact loading is performed by setting an initial velocity to the projectile along the y axis. Fixed boundary conditions are fully defined for the composite plate along its periphery, with all freedoms constrained to zero to replace the practical conditions. "Surface to Surface Contact" is used to define the contact response between the projectile and the composite plate. The penalty contact method with a finite sliding formulation is selected to calculate the contact force during the ballistic penetration process.

4.3 Structural parameters and material parameters

In this paper, the braiding pattern of the braided composite target plate is $[36 \times 6]$, thus, the interior, surface and corner unit-cells account for 57.32 %, 40.04 % and 2.64 % of the whole target. The length, width and thickness of the target are 80mm, 32mm and 4mm, respectively. The braiding angle α is 25° , braiding pitch h is 3.20mm, fiber volume fraction V_f is 50.62%. The stiffness and strength properties of fiber and matrix are listed in Table 1. The viscoelastic properties and relaxation time of matrix cited from reference [29] are summarized in Table 2.

4.4 Material degradation and element deletion

The failure criteria describe typical failure modes of 3D braided composites during ballistic penetration process. When failure occurs, materials lose their load carrying capacity in certain modes thus the corresponding mechanical properties need to be degraded. The break of braiding yarn is known to be a sudden event, therefore, in the present study, an instantaneous elastic constants reduction scheme (shown in Table 3), is introduced as the degradation model. Compared to gradual degradation scheme, the superiority of this instantaneous degradation scheme is easy for implementation and efficient for computation.

Furthermore, if a certain braiding yarn in an element loses its load carrying capacity in axial direction, the element would be removed from the finite element model.

4.5 Numerical analysis process

During each time increment, ABAQUS transmits the information of strain increment and strain rate to VUMAT. With the iso-strain assumption, the global strain increment and strain rate of the unit-cell is transformed into the local coordinates of yarns and matrix. With the rate-dependent constitutive model, the local stresses in each yarn and matrix of the unit-cell can be obtained. Once the failure criterion is satisfied, the material properties degradation is carried out by using instantaneous stiffness degradation scheme. Afterwards, the global stresses at the integration points of the elements are computed by the homogenization method mentioned above. Finally, the updated stresses and other state variables are returned to ABAQUS for next step analysis. Fig. 8 presents the flow chart of the whole numerical analysis process.

5 Results and discussion

5.1 Velocity and contact force curves

For the high velocity impact simulation of 3D braided composite target penetrated by spherical projectile and flat projectile, the initial impact velocity is set as 400 m/s. The velocity-time curve and contact force-time curve of the projectile in ballistic penetration process are shown in Fig. 9. It can be seen that the spherical projectile's velocity changes smoothly while the velocity-time curve of flat projectile has uneven steps. The impact contact force of the spherical projectile has a large peak value at $t=8.5\mu\text{s}$, but the impact force is relatively small. On the contrast, the impact contact force of the flat projectile has multiple peak values and the impact forces are relatively large. The variations of projectile's velocity and impact contact force in the ballistic impact process are determined by many factors: the contact condition between the projectile and target, material failure time, material damage modes and elements deletion.

5.2 Simulation of high velocity impact penetration process

High velocity impact is known as a transient dynamic behavior. The ballistic penetration mechanisms in 3D textile composite structure are very complicated; however, they can be illustrated in detail by finite element simulation. Fig. 10 demonstrates the ballistic penetration process of the spherical projectile in the braided composite target. It can be seen that within $30\mu\text{s}$, the spherical projectile has completely passed through the composite plate. With the duration of impact, various failure modes occur, promote and couple with each other. The whole penetration process can be divided into three periods. (a) Opening punching period which happens in the front side of composite target at the initiation of the penetration development, as shown in Fig. 10(a), Fig. 10(b) and Fig. 10(c). When the projectile touch the front surface of the target, the compression stress wave is generated and spread quickly along the axial and transverse directions of the material. In the impact contact zone, the fiber crushing fracture and shear failure occur, thus the element in the contact zone are removed. The spherical concave shape is formed on the front surface of the target plate, and no obvious deformation happens on the back side of the target plate in this period. (b) Back fiber breaking period. In this period, the perforation ability of the projectile has been reduced due to the energy absorption during punching failure. However, as shown in Fig. 10(d) and Fig. 10(e), with the penetration depth increasing, the elements under the impact zone of the target are removed gradually, and the bending deformation on the back of the target increases. Fiber tension breaking occurs and expands outward gradually. (c) Projectile penetration and damage propagation period. As shown in Fig. 10(f), the projectile and the target plate are no longer in contact, that is, the target has penetrated completely and the velocity of the projectile is no longer changes. In this period, the compression wave in the target arrives at the free surface of the material and reflects back as the tension wave. With the interaction of tension and compression wave, new damage (mainly matrix damage) emerges continuously for a while.

Figure 11 presents the ballistic penetration process of the flat projectile into the braided composite target. The whole process costs about $55\mu\text{s}$. Similarly, the penetration process can be summarized as three periods: opening punching, back fiber breaking and projectile penetration (damage propagation) period. As shown in Fig. 11(a), Fig. 11(b) and Fig. 11(c), when the flat projectile contacts the target plate, fiber tension and shear fracture damage are generated in a circle shape in the contact zone between the projectile's head and the target plate. The fiber compression fracture is formed in the contact zone between the flat surface of the projectile and the target plate. These failed elements are deleted to form a cylindrical concave on the front surface of the target plate. At this time, the back of the target plate is less deformed. As shown in Fig. 11(d), with the penetration process continues, the deformation of the back of the target plate is gradually increased. Convex phenomenon appears and the fiber tension fracture occurs in the convex zone and expands outward gradually. As shown in Fig. 11(e) and Fig. 11(f), the materials on the back side of the target collapse and the target plate penetrated. Material pieces generated in the ballistic impact process splash out of the projectile holes. After $t > 11.5\mu\text{s}$, the projectile and target plate are separated. The projectile continues to move at a constant velocity until it is completely moves away from the target. In this period, the deformation of target plate recovered gradually. However, with the interaction of tension and compression stress waves, the target plate continues to produce certain modes of damage, mainly the matrix damage.

5.3 Damage modes analysis

The main failure modes of 3D braided composite target under high velocity impact include yarn axial breaking,

yarn tension and compression in transverse direction, yarn shear failure and matrix cracking. Among them, yarn axial breaking control the final penetration of the composite target. Although other damage modes will not lead to the perforation of the target plate directly, they have important effects on the ballistic impact damage process and the residual strength of the target plate. Enough attention should also be paid to these damage modes.

Figure 12 describes the yarn compression failure and matrix damage of the braided composite target under the penetration of the spherical projectile. The black area represents the corresponding damage mode. The evolution of yarn compression failure in the key influence area on the front surface of the target plate is given in Fig. 12(a). When the projectile reaches the target plate, the yarn compression failure occurs in the contact area. With the impact process continues, the contact area increases. That is, the damage area and the number of damaged elements increase. After $t > 10\mu\text{s}$, half of the spherical projectile has penetrated into the target plate. The damage area on the surface of the target plate is no longer increased anymore. Fig. 12(b) displays the evolution of matrix damage on the target front surface. The matrix damage is appeared in the contact area of the projectile and the target plate first. As the penetration depth increases, the matrix damage increases on the outer surface of the target plate and extends outward along the in-plane directions of the target plate. After the target plate penetration, the area which is far away from the contact area of the target plate continues to produce new matrix damage under the action of stress wave.

Figure 13 illustrates the yarn tension, compression and shear failure and matrix damage of the braided composite target under the penetration of the flat projectile. Fig. 13(a) and Fig. 13(b) present the yarn tension and compression failure in the key influence area at $t = 0.5\mu\text{s}$. Due to the shear punching effect of the projectile's edge on the target plate, a circle of yarn tension damage elements appear in the contact zone. At the same time, because of the compression punching effect of the projectile flat head on the target plate, yarn compression damage elements occur with approximately equivalent area of the head surface of the projectile. Fig. 13(c) demonstrates the shear damage distribution in the vertical contact surface direction of the projectile penetrating the target. The yarn compression and shear failure elements in the horizontal contact surface direction are deleted thus not shown here. In the ballistic penetration process, under the action of stress wave, the number of shear damage elements increase slightly, but the quantity is relatively small. Fig. 13(d) presents the evolution of matrix damage on the target front surface. At $t = 0.5\mu\text{s}$, the area of matrix damage is approximately equivalent to the head surface area of the projectile. As the penetration depth increases, the matrix damage appears on the target plane near the contact zone and extends outward along the in-plane directions of the target plate.

5.4 Effect of striking velocity on the residual velocity and target energy absorption

According to the energy conservation law, the kinetic energy loss of projectile after penetrating the target plate is:

$$E_k = \frac{1}{2} m (V_0^2 - V_r^2) \quad (24)$$

where V_0 is the initial striking velocity, V_r is the residual velocity.

Ignoring the energy dissipation in the ballistic impact process, the loss of the projectile's kinetic energy is approximately equal to the energy absorption value of the target plate. Fig. 14 shows the variation of residual velocity and energy absorption with striking velocity. It is clearly seen from Fig. 14(a) that the residual velocity

increases linearly with the increase in the impact velocity. Fig. 14(b) exhibits that the target energy absorption increases monotonically with the increasing of the impact velocity, but it is not a linear relationship. It is also seen that the residual velocity of the flat projectile is smaller than spherical projectile, and the energy absorption of the target plate is significantly larger than that of the spherical projectile with the same initial striking velocity.

6 Conclusions

Ballistic impact numerical simulation can save expensive costs of material specimen and impact test, obtain the data which is difficult to be measured in the experiment, and provide more information on the damage characteristics in the penetration process. In this paper, 3D braided composite target plate under ballistic impact is selected as the research object. Based on the 3D rate-dependent damage constitutive model of constituents and the three unit-cells model of the composite structure, a finite element model of impact damage analysis is established. Tsai-Wu and Mises criteria are adopted as damage initiation criteria of yarns and matrix, respectively. By using an instantaneous degradation scheme to implement the stiffness reduction, the whole process of damage evolution is simulated and the damage mechanisms are revealed in detail. Element deletion is introduced in the simulation process to ensure residual stiffness to prevent excessive element distortion.

The study shows that the penetration process can be summarized as three periods: opening punching, back fiber breaking and projectile penetration (damage propagation) period. The main failure modes of 3D braided composite target include yarn axial breaking, yarn tension and compression in transverse direction, yarn shear failure and matrix cracking. It is also exhibited that there is a nearly linear relationship between the residual velocity and the striking velocity of the projectile, and the energy absorption of the target plate increases with the increase of the striking velocity while it is not a linear relationship. The finite element model developed in this paper can be used to impact damage resistant design of 3D braided composites and the survivability design of the aircraft composite structures.

Acknowledgements

The authors of this paper wish to acknowledge the financial support by Postdoctoral Science Foundation of Jiangsu Province (1402101C) and Senior Talent Start-up Foundation of Jiangsu University (14JDG136).

References

- [1] Yang JM, Ma CL and Chou TW. Fiber inclination model of three dimensional textile structural composites. *J Compos Mater* 1986; 20(5): 472-484.
- [2] Mohajerjasbi S. Structure and mechanical properties of 3D braided composites. Ph. D thesis, Drexel University, US, 1993.
- [3] Wang YQ and Wang ASD. Microstructure/property relationships in three dimensionally braided fiber composites. *Compos Sci Technol* 1995; 53(2): 213-232.
- [4] Chen L, Tao XM and Choy CL. On the microstructure of three-dimensional braided preforms. *Compos Sci Technol* 1999; 59(3): 391-404.
- [5] Sun HY and Qiao X. Prediction of mechanical properties of three-dimensionally braided composites. *Compos Sci Technol* 1997; 57(6): 623-629.
- [6] Sun XK and Sun CJ. Mechanical properties of three-dimensional braided composites. *Compos Struct* 2004; 65(3-4): 485-492.
- [7] Yu XG and Cui JZ. The prediction on mechanical properties of 4-step braided composites via two-scale method.

- Compos Sci Technol* 2007; 67(3-4): 471-80.
- [8] Zhang C and Xu XW. Finite element analysis of 3D braided composites based on three unit-cells models. *Compos Struct* 2013; 98: 130-142.
- [9] Zeng T, Wu LZ and Guo LC. A finite element model for failure analysis of 3D braided composites. *Mater Sci Eng A* 2004; 366(1): 144-151.
- [10] Dong JW and Feng ML. Asymptotic expansion homogenization for simulating progressive damage of 3D braided composites. *Compos Struct* 2010; 92(4): 873-882.
- [11] Fang GD, Liang J and Wang BL. Effect of interface properties on mechanical behavior of 3D four directional braided composites with large braid angle subjected to uniaxial tension. *Appl Compos Mater* 2011; 18(5): 449-465.
- [12] Zhang DT, Sun Y, Wang XM, et al. Meso-scale finite element analyses of three-dimensional five-directional braided composites subjected to uniaxial and biaxial loading. *J Reinf Plast Comp* 2015; 34(24): 1989-2005.
- [13] Gong JC and Sankar BV. Impact properties of three-dimensional braided graphite/epoxy composites. *J Compos Mater* 1991; 25(6): 715-731.
- [14] Flanagan MP, Zikry MA, Wall JW et al. An experimental investigation of high velocity impact and penetration failure modes in textile composites. *J Compos Mater* 1999; 33(12): 1080-1103.
- [15] Xu J and Gu BH. Damage pattern and failure mode of 3-dimensional composites under ballistic impact. *J Ballist* 2002; 14(2): 39-43.
- [16] Wen HM. Predicting the penetration and perforation of FRP laminates struck normally by projectiles with different nose shapes. *Compos Struct* 2000; 49(3): 321-329.
- [17] Naik NK and Shirao P. Composite structures under ballistic impact. *Compos Struct* 2004; 66(1-4): 579-590.
- [18] Udatha P, Kumar CVS, Nair NS, Naik N K. High velocity impact performance of three-dimensional woven composites. *J Strain Anal Eng Des* 2012; 47(7): 419-431.
- [19] Jenq ST and Mao JJ. Ballistic impact response for two-step braided three dimensional textile composites. *AIAA Journal* 1996; 34(2): 375-384.
- [20] Jenq ST, Kuo JT and Sheu LT. Ballistic impact response of 3D four-step braided glass/epoxy composites. *Key Eng Mater* 1998; 141-143(1): 349-366.
- [21] Gu B and Ding X. A refined quasi-microstructure model for finite element analysis of three dimensional braided composites under ballistic penetration. *J Compos Mater* 2005; 39(8): 685-710.
- [22] Ji KH and Kim SJ. Dynamic direct numerical simulation of woven composites for low-velocity impact. *J Compos Mater* 2007; 41(2): 175-200.
- [23] Gu B. A microstructure model for finite-element simulation of 3D rectangular braided composite under ballistic penetration. *Philos Magaz* 2007; 87(30): 4643-4669.
- [24] Bahei-El-Din YA, Zikry MA. Impact induced deformation fields in 2D and 3D woven composites. *Compos Sci Technol* 2003; 63(7): 923-942.
- [25] Zhang Y, Jiang L L, Sun B Z, et al. Transverse impact behaviors of four-step 3-D rectangular braided composites from unit-cell approach. *J Reinf Plast Comp* 2012; 31(4): 233-246.
- [26] Sun BZ, Liu YK and Gu BH. A unit cell approach of finite element calculation of ballistic impact damage of 3-D orthogonal woven composite. *Compos Part B* 2009; 40(6): 552-560.
- [27] Li ZJ, Sun BZ and Gu B. FEM simulation of 3D angle-interlocked woven composite under ballistic impact from unit cell approach. *Comput Mater Sci* 2010; 49(1): 171-183.
- [28] Tang YY, Sun BZ and Gu BH. Impact damage of 3D cellular woven composite from unit-cell level analysis. *Int J Damage Mech* 2011; 20(3): 323-346.
- [29] Karim MR and Hoo fatt MS. Rate-dependent constitutive equations for carbon fiber-reinforced epoxy. *Polym Compos* 2006; 27(5): 513-528.
- [30] Chamis C C. Mechanics of Composites Materials: Past, Present and Future. *J Compos Technol Res* 1989; 11(1): 3-14.

List of Figure Captions

Fig. 1 x - y plane projection of all the yarn traces

Fig. 2 Topology geometrical and structural models of three unit-cells (a) Interior unit-cell (b) Surface unit-cell (c) Corner unit-cell

Fig. 3 Constitutive model of the fiber and matrix (a) linear-elastic (b) viscoelastic

Fig. 4 Constitutive model of unidirectional composite in longitudinal direction

Fig. 5 Local coordinate definition of the braiding yarn

Fig. 6 Region division of the 3D braided composite target plate

Fig. 7 Finite element model of high velocity impact damage analysis (a) Spherical projectile (b) Flat cylindrical projectile

Fig. 8 Flow chart for ballistic damage analysis process

Fig. 9 Velocity-time curve and contact force-time curve of the projectiles (a) Velocity-time curve of spherical projectile (b) Contact force-time curve of spherical projectile (c) Velocity-time curve of flat projectile (d) Contact force-time curve of flat projectile

Fig. 10 Ballistic penetration process of the spherical projectile in the target plate (a) $t=1\mu\text{s}$ (b) $t=3\mu\text{s}$ (c) $t=6\mu\text{s}$ (d) $t=8\mu\text{s}$ (e) $t=10\mu\text{s}$ (f) $t=30\mu\text{s}$

Fig. 11 Ballistic penetration process of the flat projectile in the target plate (a) $t=1\mu\text{s}$ (b) $t=3\mu\text{s}$ (c) $t=6\mu\text{s}$ (d) $t=8\mu\text{s}$ (e) $t=11\mu\text{s}$ (f) $t=40\mu\text{s}$

Fig. 12 Damage mode of the target plate under the penetration of spherical projectile (a) Yarn compression failure (b) Matrix damage

Fig. 13 Damage mode of the target plate under the penetration of flat projectile (a) Yarn tension failure (b) Yarn compression failure (c) Yarn shear failure (d) Matrix damage

Fig. 14 Variation of residual velocity and energy absorption with striking velocity of the projectile (a) Residual velocity- striking velocity curve (b) Energy absorption-striking velocity curve

List of Table Titles

Table 1 Stiffness and strength properties of fiber and matrix

Table 2 Viscoelastic properties and relaxation time of matrix

Table 3 Stiffness reduction scheme

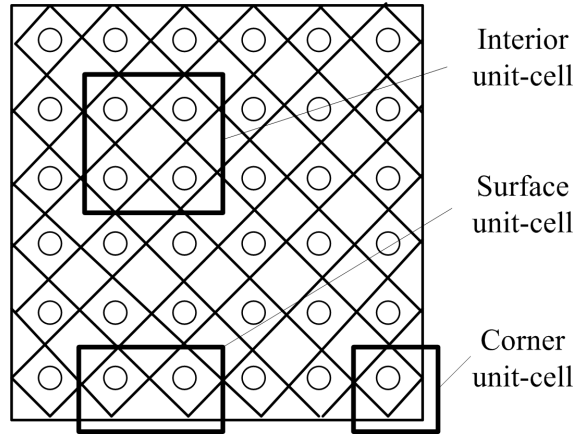


Fig. 1 x - y plane projection of all the yarn traces

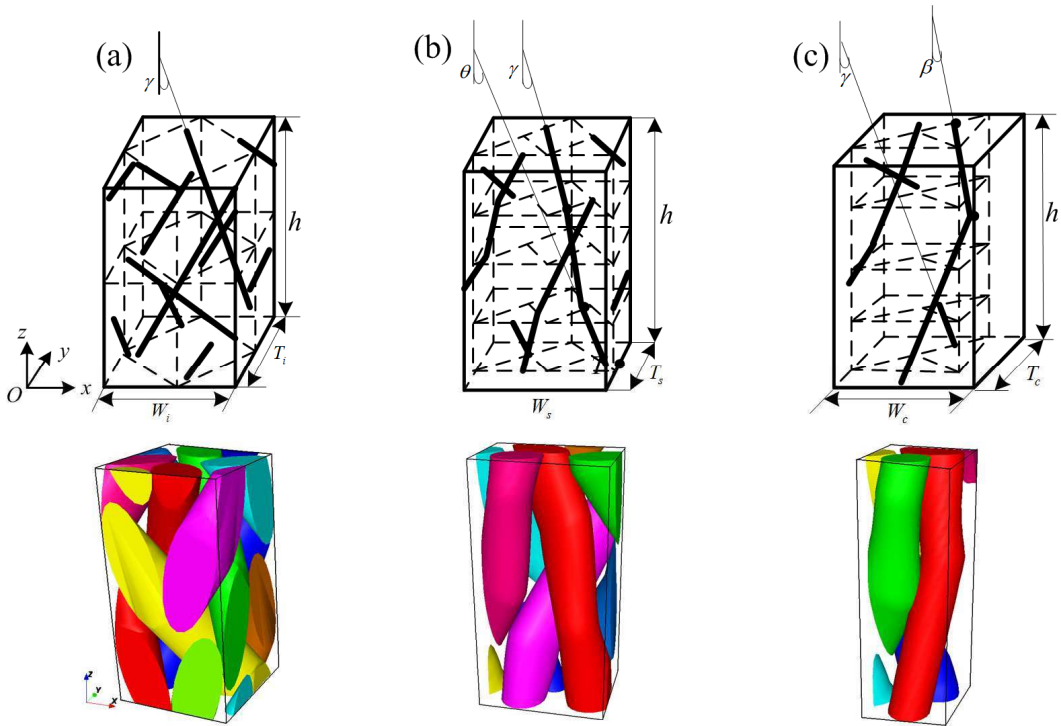


Fig. 2 Topology geometrical and structural models of three unit-cells (a) Interior unit-cell (b) Surface unit-cell (c) Corner unit-cell

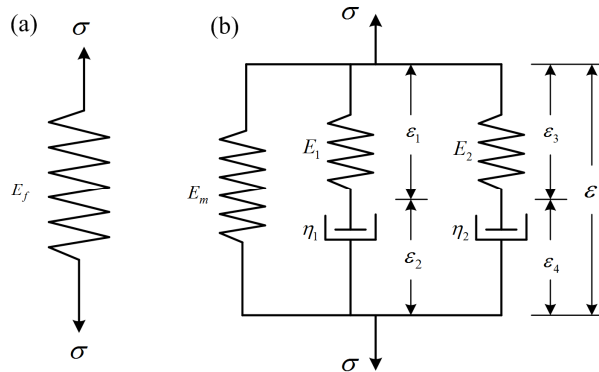


Fig. 3 Constitutive model of the fiber and matrix (a) linear-elastic (b) viscoelastic

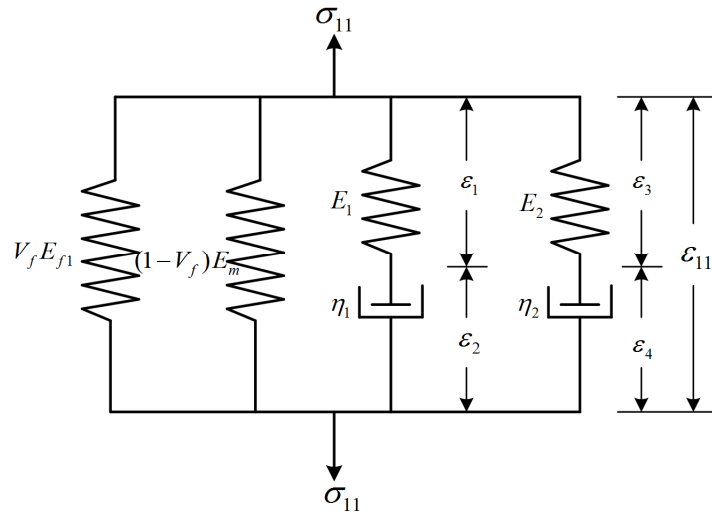


Fig. 4 Constitutive model of unidirectional composite in longitudinal direction

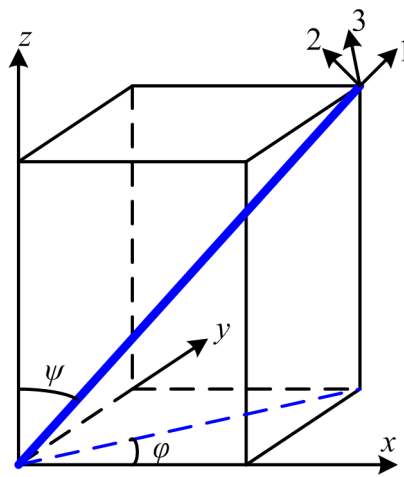


Fig. 5 Local coordinate definition of the braiding yarn

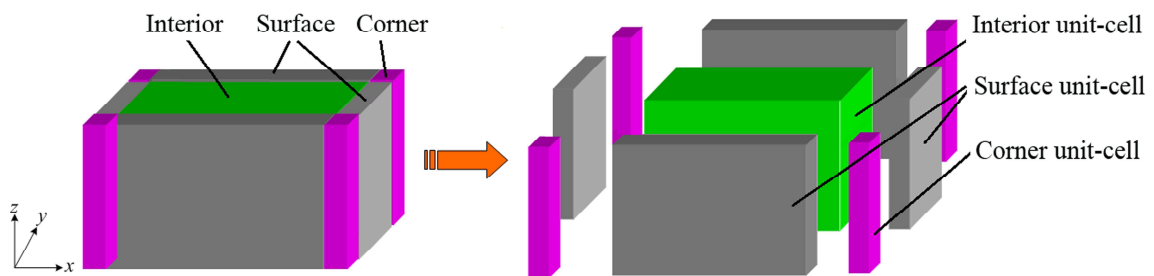


Fig. 6 Region division of the 3D braided composite target plate

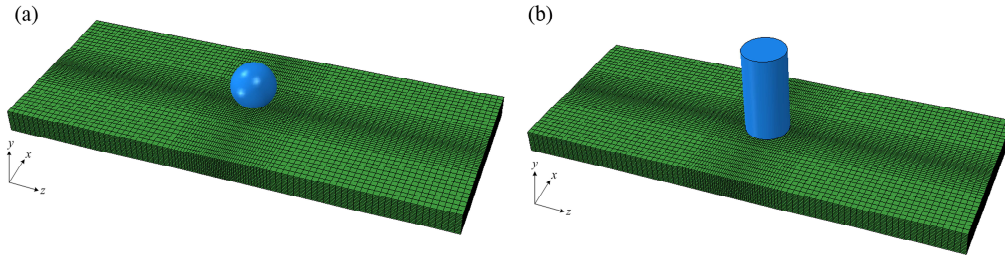


Fig. 7 Finite element model of high velocity impact damage analysis (a) Spherical projectile (b) Flat cylindrical projectile

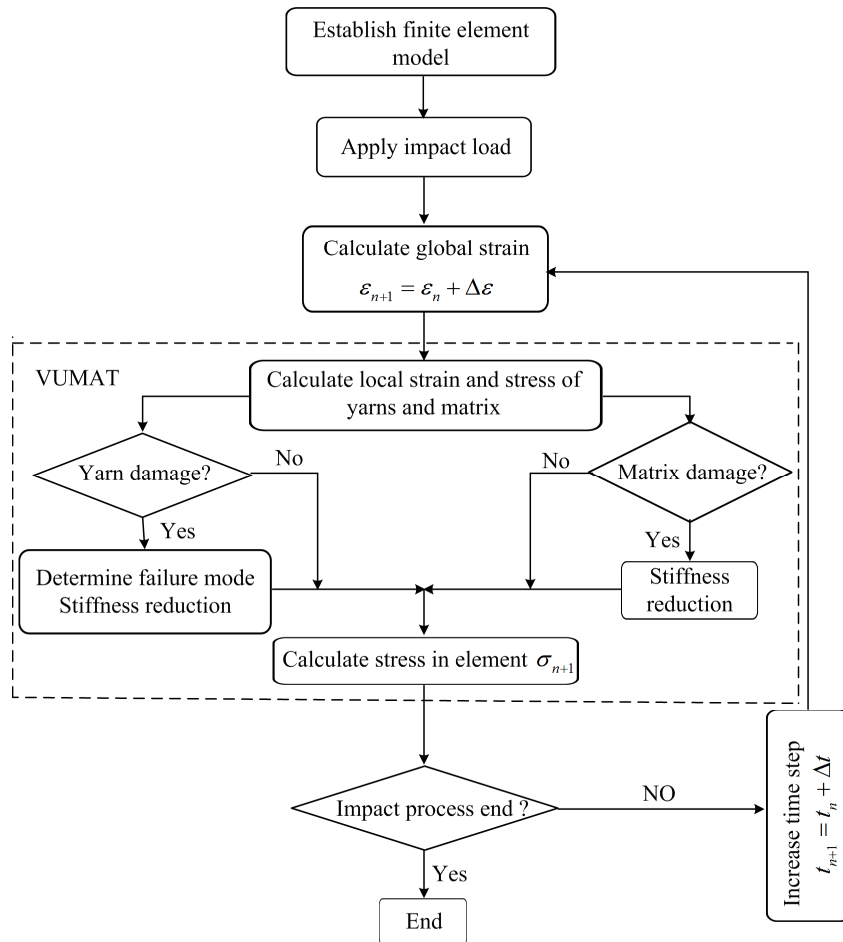


Fig. 8 Flow chart for ballistic damage analysis process

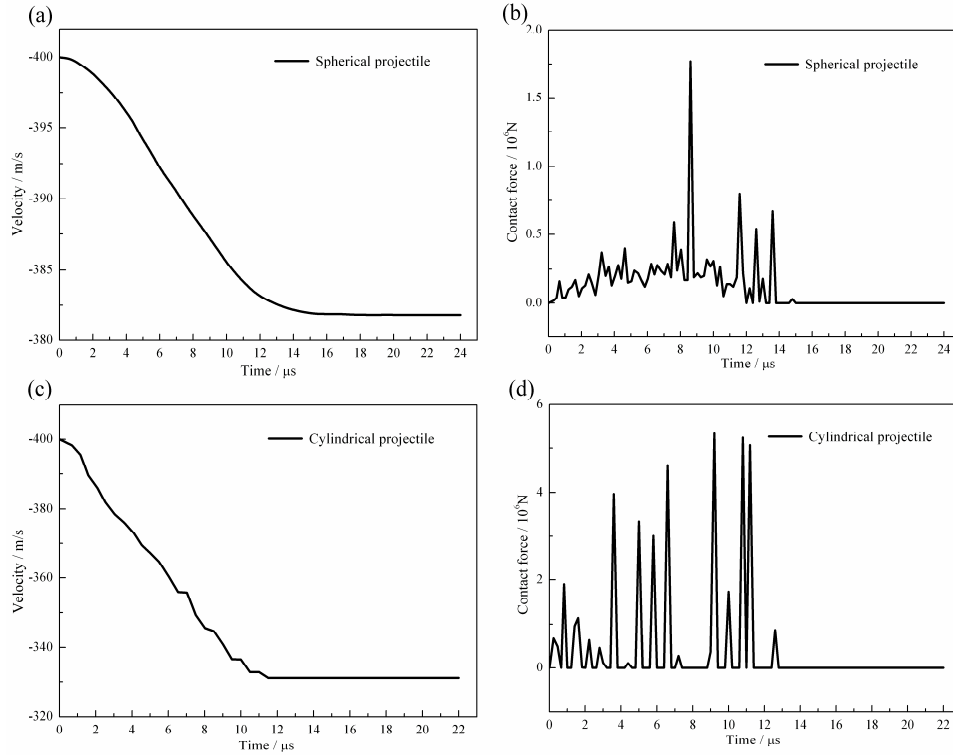


Fig. 9 Velocity-time curve and contact force-time curve of the projectiles (a) Velocity-time curve of spherical projectile (b) Contact force-time curve of spherical projectile (c) Velocity-time curve of flat projectile (d) Contact force-time curve of flat projectile

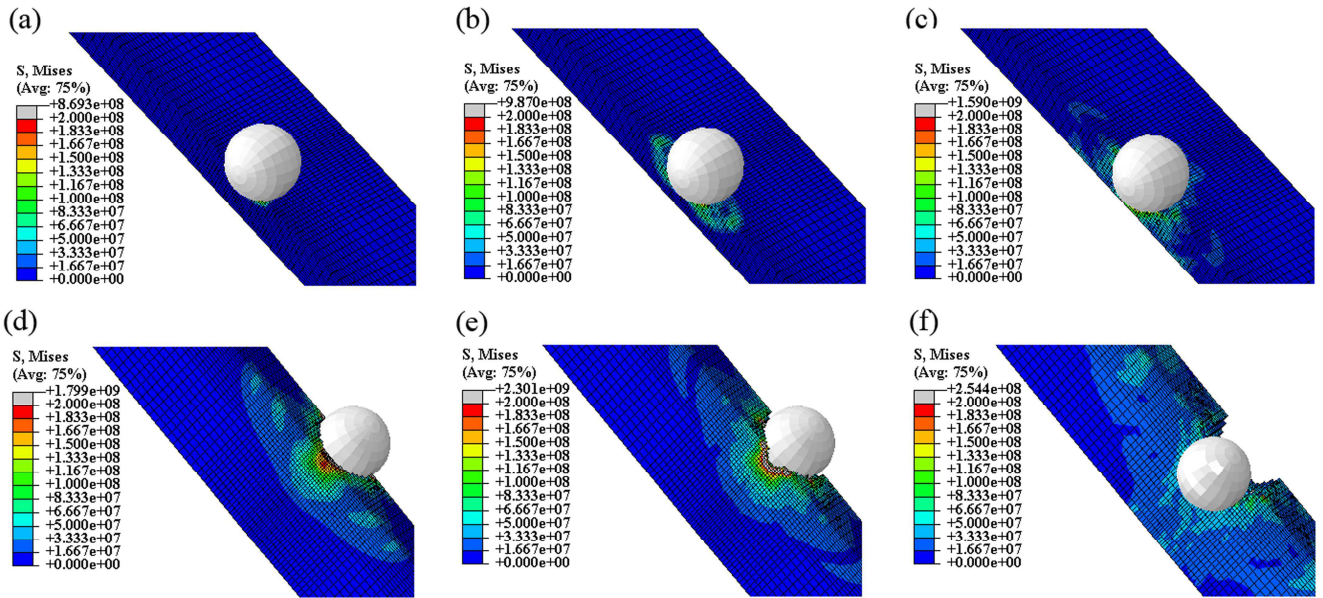


Fig. 10 Ballistic penetration process of the spherical projectile in the target plate (a) $t=1\mu\text{s}$ (b) $t=3\mu\text{s}$ (c) $t=6\mu\text{s}$ (d) $t=8\mu\text{s}$ (e) $t=10\mu\text{s}$ (f) $t=30\mu\text{s}$

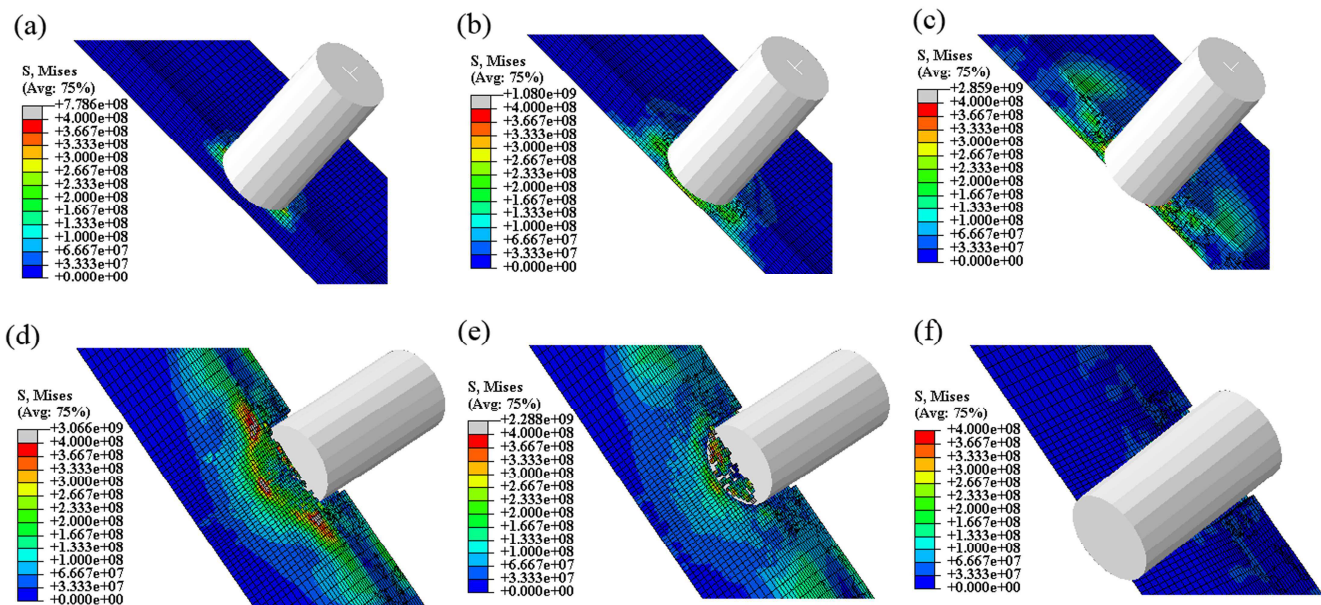


Fig. 11 Ballistic penetration process of the flat projectile in the target plate (a) $t=1\mu\text{s}$ (b) $t=3\mu\text{s}$ (c) $t=6\mu\text{s}$ (d) $t=8\mu\text{s}$ (e) $t=11\mu\text{s}$ (f) $t=40\mu\text{s}$

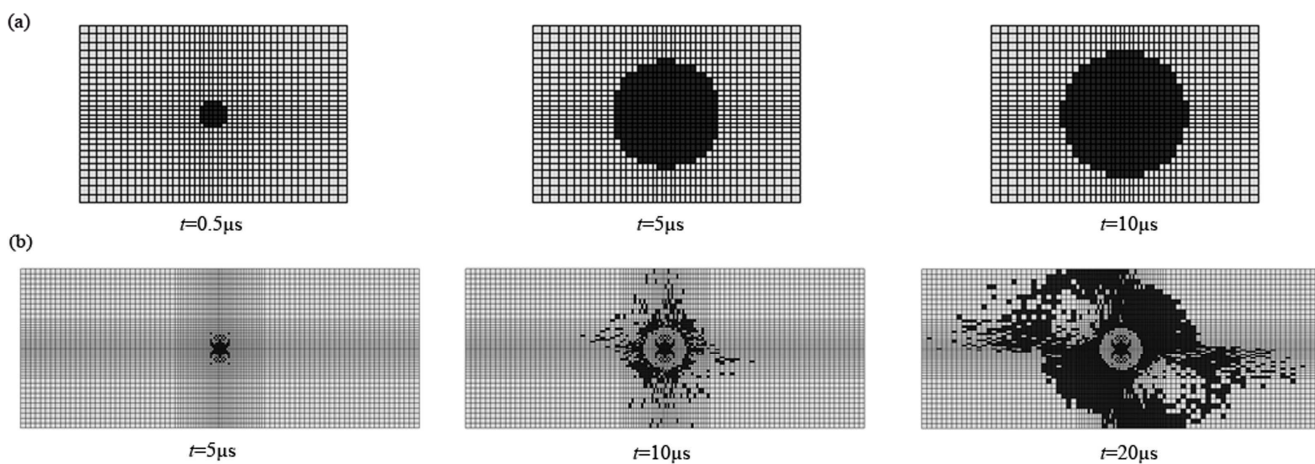


Fig. 12 Damage mode of the target plate under the penetration of spherical projectile (a) Yarn compression failure (b) Matrix damage

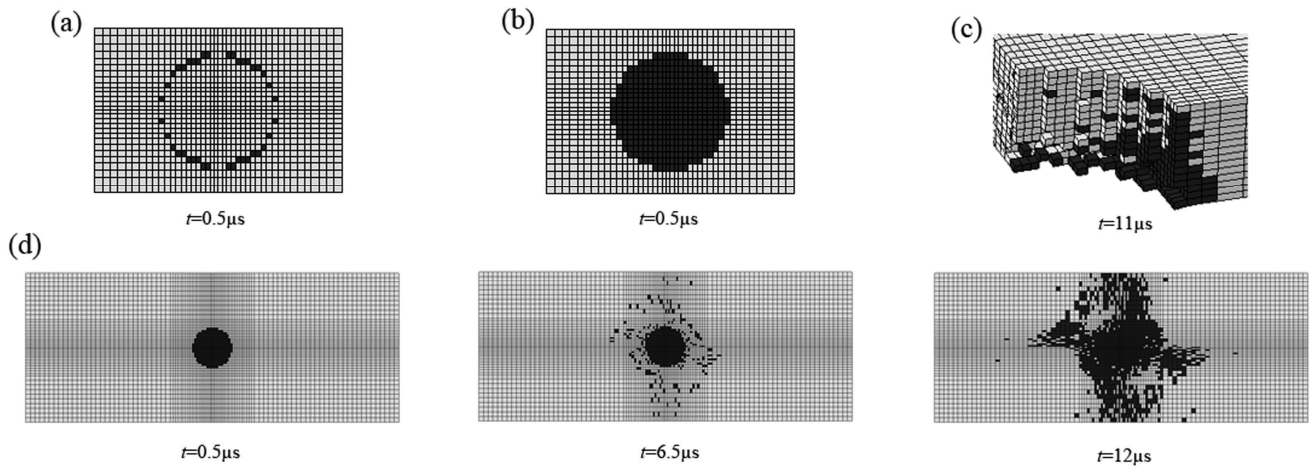


Fig. 13 Damage mode of the target plate under the penetration of flat projectile (a) Yarn tension failure (b) Yarn compression failure (c) Yarn shear failure (d) Matrix damage

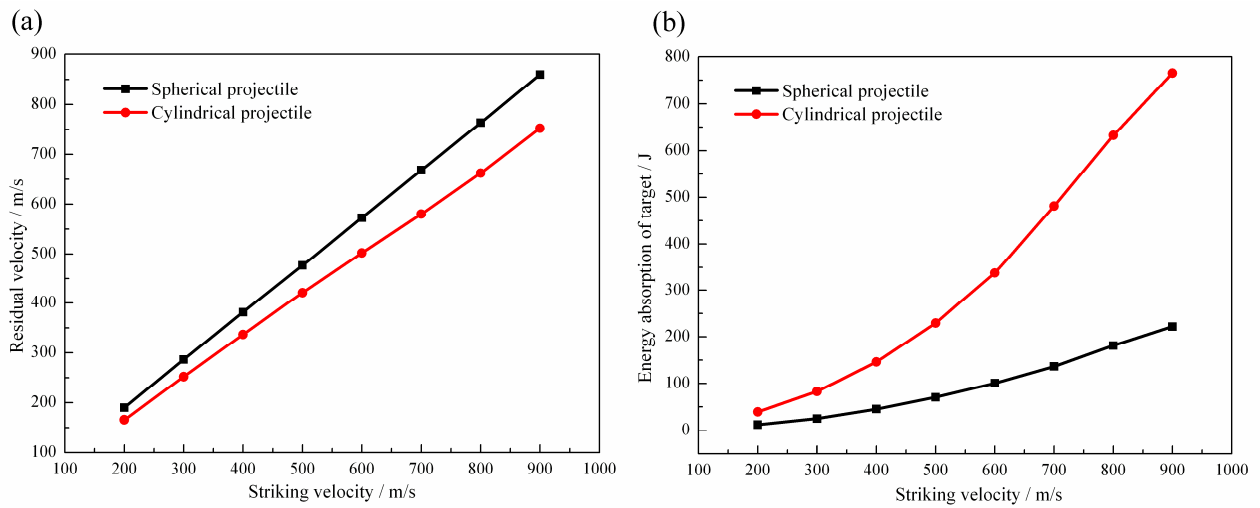


Fig. 14 Variation of residual velocity and energy absorption with striking velocity of the projectile (a) Residual velocity- striking velocity curve (b) Energy absorption-striking velocity curve